**Organic field effect transistors based on ternary blends including a fluorinated polymer for achieving enhanced device stability**

*Adrián Tamayo*[a], *Tommaso Salzillo*[a,⊥], *Marta Mas-Torrent* [a]*

[a] Institut de Ciència de Materials de Barcelona (ICMAB-CSIC), Campus de la UAB, 08193 Bellaterra, Barcelona, Spain.
[⊥] Current address: Department of Chemical and Biological Physics, Weizmann Institute of Science, Herzl street 234, 76100 Rehovot, Israel.
E-mail: mmas@icmab.es

Keywords: OFETs, solution shearing, device stability, printed electronics.

The stability of organic semiconductors (OSCs) is strongly hampered by the presence of water molecules. One approach that has been proved to lead to organic field-effect transistors with an enhanced performance is the use of blends of OSCs with insulating binding polymers. In this work, we report the fabrication of OSC thin films based on polymeric ternary blends including a hydrophobic fluorinated polymer as a novel route to engineer long-term reliable OFET devices. In particular, we explore here the fabrication of OFETs based on blends of bis(triisopropylsilylethynyl)pentacene (TIPS) with polystyrene (PS) and poly(pentafluorostyrene) (PFS). The PS:PFS ratio is tuned in order to find the optimum formulation. It is shown that films including 20% of PFS in the polymeric blend exhibit an improved device performance, which is reflected by a low bias stress and an exceptional environmental stability, without significantly hampering the OFET mobility. Our work advocates that adding a small percentage of fluorinated polymers in OSC blends is a promising route to realise more reliable and stable devices without importantly compromising the device mobility.

## 1. Introduction

The performance of printed organic field-effect transistors (OFETs) has significantly improved over the last few years making them highly appealing for large-area and low-cost applications.[1,2] However, although in the last few years an enhancement in the devices stability has been achieved,[3–5] still one of the main bottlenecks hindering their practical implementation is their limited stability over time and under continuous operation. OFETs are based on the formation of a conductive channel at the semiconductor/dielectric interface upon the application of an electric field. Although the organic semiconductor (OSC) is the active layer in the device, since charge transport takes place at the first few OSC molecular layers near the gate dielectric, this interface significantly determines the overall device properties. Water molecules penetrating into the OSC layer are detrimental to the device performance.[3,5] Further, surface dipoles at the dielectric interface, such as the hydroxyl groups of the most commonly used $SiO_2$ dielectric, can trap injected charges and lead to hysteresis, a mobility decrease and a significantly reduced bias stress stability.[6]

In order to circumvent these effects, different approaches have been followed. In bottom-gated devices, the passivation of the dielectric with hydrophobic self-assembled monolayers or polymer layers has been often pursued.[6–11] Particularly appealing, is the use of fluorinated polymers since they are highly hydrophobic and their deep highest occupied molecular orbital (HOMO) level provides a large barrier for charge trapping.[12,13] Furthermore, the use of gate dielectrics based on fluorinated polymers has also been proved to be a useful strategy to achieve devices with improved bias stress stability.[11,14–16] However, the coating of the OSC from solution on such hydrophobic layers can be challenging and also the OSC crystallisation on the surface can be hindered. Regarding the OSC environmental protection, top encapsulation layers have been employed to avoid water and oxygen penetration, including also fluorinated polymers such as Cytop.[5,17–20] Recently, the use of additives within the organic semiconductor layer has also been successfully applied to displace water and enhance

the device stability.[3,21] With the aim at facilitating the processing of OSCs and achieve large-area uniform coatings, several groups have been working on the preparation of films based on blends of OSCs with an insulating polymer matrix.[22–28] Importantly, this methodology often leads to films with an enhanced crystallinity, a higher environmental stability and a reduced number of interfacial traps at the semiconductor/dielectric interface. This has been attributed to the vertical phase separation that takes place during crystallisation that leads to a crystalline OSC film sitting on top of an insulating polymer layer which acts as a passivation coating.[29–31] However, the potential of using fluorinated polymers in this strategy has hardly been explored,[32] probably due to their constrained compatibility with the OSC.

In this work, we report the fabrication of OSC thin films based on polymeric ternary blends including a fluorinated polymer as an efficient route to engineer long-term reliable OFET devices under atmospheric conditions. As active material the benchmark OSC 6,13-Bis(triisopropylsilylethynyl)pentacene (TIPS) was selected, which was blended with polystyrene (PS) and poly(pentafluorostyrene) (PFS) (**Figure 1a**). By tuning the PS:PFS ratio an optimised device OFET performance was achieved, which was reflected by a low bias stress and an improved environmental stability, without importantly compromising the OFET mobility.

## 2. Results and Discussion

Solutions of TIPS:Polymer (4:1) in chlorobenzene 2 % wt. were prepared as previously reported.[33] However, in this case, mixtures of PS with PFS were employed as binding polymer with the following PS:PFS proportions: 1:0, 4:1, 3:2, 2:3, 1:4, 0:1. From now on, we call after these mixtures as $PS_{1.0}PFS_0$, $PS_{0.8}PFS_{0.2}$, $PS_{0.6}PFS_{0.4}$, $PS_{0.4}PFS_{0.6}$, $PS_{0.2}PFS_{0.8}$ and $PS_0PFS_{1.0}$. These solutions were deposited by Bar-Assisted Meniscus Shearing (BAMS) on $Si/SiO_2$ substrates with interdigitated gold electrodes at a coating speed of 10 mm/s and at a stage temperature of 105 ºC (for details see experimental section). Such technique has been

proved to give rise to homogenous and crystalline large area thin films with high throughput (**Figure 1b**).[33,34] It should be noticed that the selected coating speed is located in an intermediate regime between the evaporation and the Landau regime.[35,36] Moving to larger speeds did not improve the device mobility, but eventually, the performance decreased (i.e., above a coating speed of 40 mm/s).[37,38]

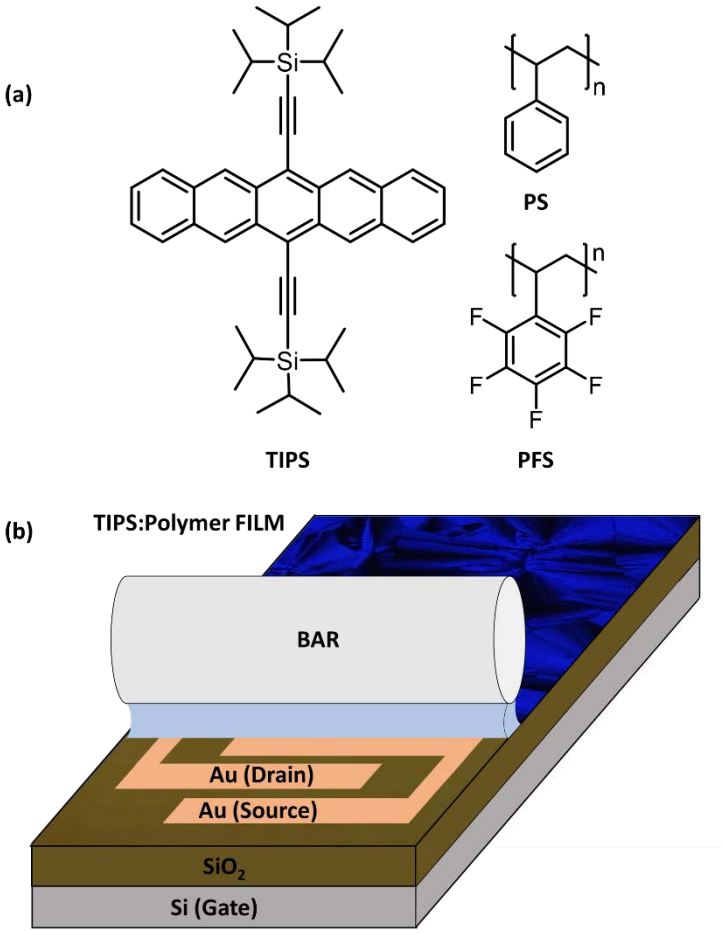


**Figure 1**. a) Molecular structures of 6,13-Bis(triisopropylsilylethynyl)pentacene (TIPS), poly(pentafluorostyrene) (PFS) and polystyrene (PS). b) Schematic illustration of the BAMS technique.

The thin films prepared with all the formulations were inspected by polarised optical microscopy (**Figure 2).** The films displayed the typical TIPS spherulitic crystallites as

previously reported.[33] It was found that the presence of PFS is not significantly affecting the film morphology, with the exception of the films based on only PFS as binding polymer, in which very small crystallites not covering the whole surface were observed (**Figure 2f**). In fact, the TIPS:$PS_0PFS_1$ ink solutions were very difficult to deposit on the substrates due to their high hydrophobicity resulting often in non-uniform and low reproducible films. For this reason, these films were not further explored.

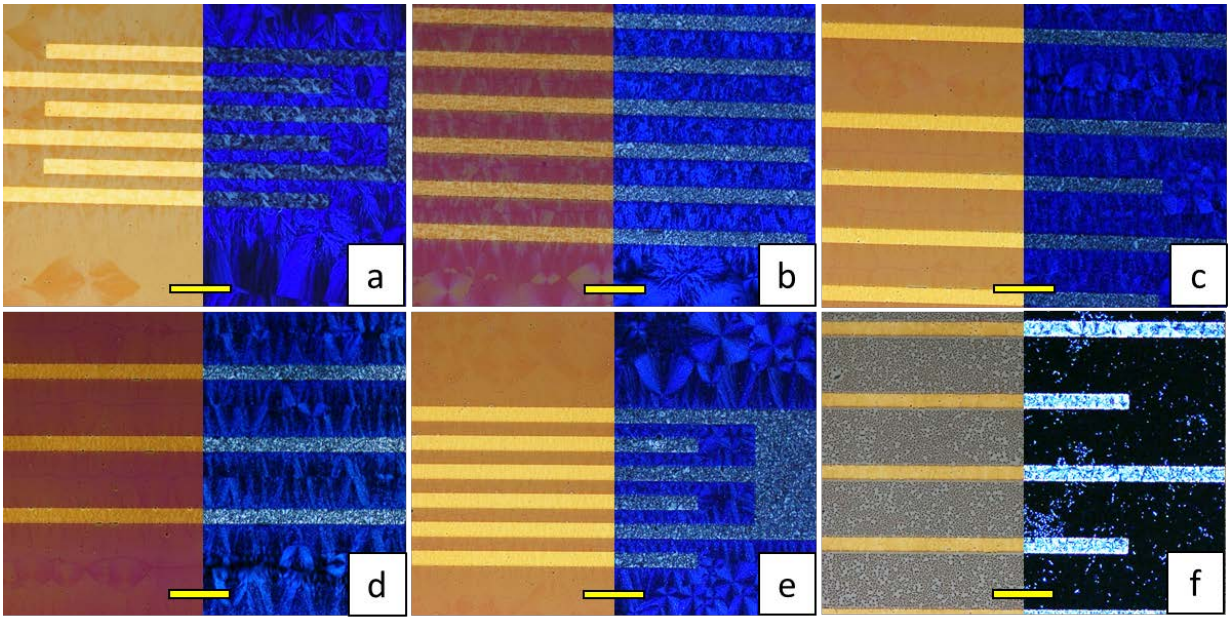


**Figure 2.** Optical microscope (left) and polarised (right) images of the prepared TIPS films blended with the following PS:PFS proportions: (a) $PS_{1.0}PFS_0$, (b) $PS_{0.8}PFS_{0.2}$, (c) $PS_{0.6}PFS_{0.4}$, (d) $PS_{0.4}PFS_{0.6}$, (e) $PS_{0.2}PFS_{0.8}$ and (f) $PS_0PFS_{1.0}$. Scale bar: 200 µm.

The films were closely explored by atomic force microscopy (AFM). The AFM topography measurements revealed that the domain size of the microcrystals in the films with PFS were smaller than the ones based on only PS **(Figure 3 and Figure S1)**. This might be caused by the lower diffusion of the OSC molecules in the PFS binder.[39] Additionally, the height distribution of the different films is influenced by the ratio PS:PFS. The normalization of the height density distribution ρ(p) (where p is the corresponding height quantity) is plotted as an inset in the AFM pictures. The films with minimum roughness, thickness and height

distribution correspond to the formulation $PS_{0.6}PFS_{0.4}$, with an average roughness (estimated by the root mean square (rms)) of 4.5±0.8 nm and thickness of 18.5±6.3 nm (**Table S1**). Noticeably, in the films based on polymeric blends with 60 % or more of PFS, small circular protruding features were observed **Figure 3 (e and g)**. We believe that this is caused by a lateral phase separation that takes place due to the lower miscibility between the two polymers when they are mixed in these percentages, leading to the formation of small PFS aggregates.[40,41]

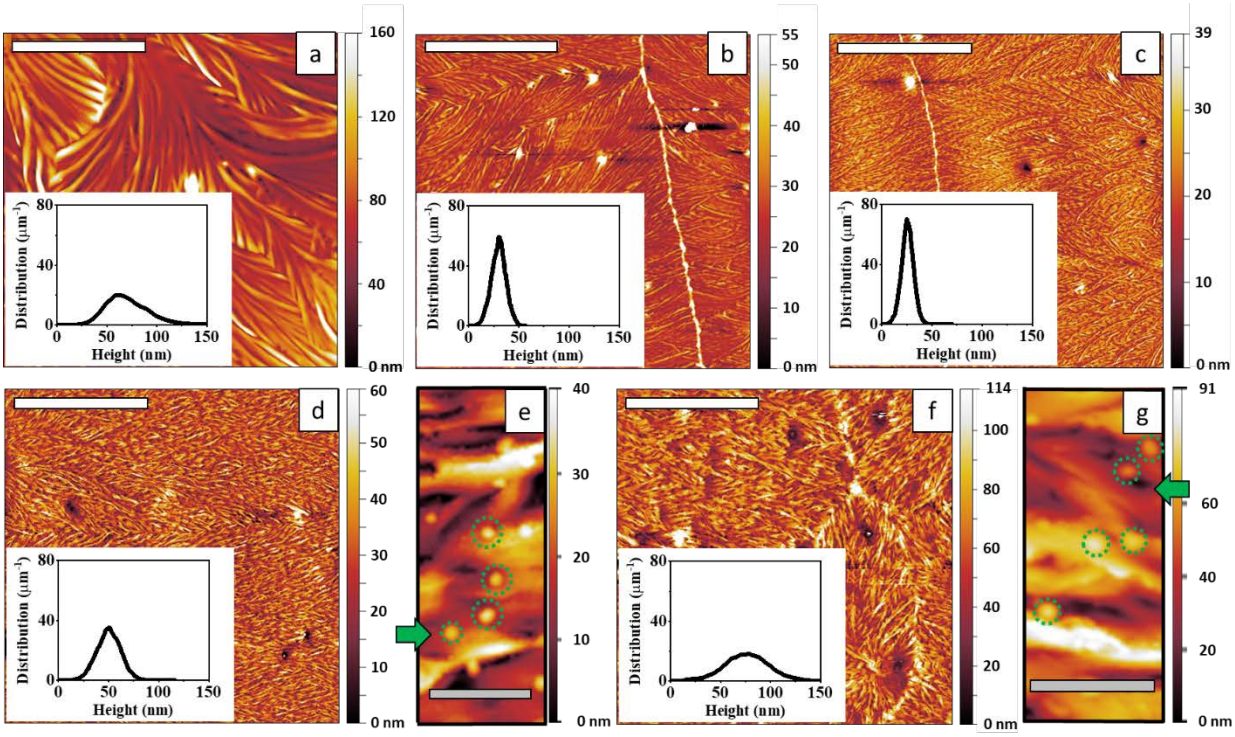


**Figure 3**. Topographical AFM images of TIPS thin films deposited using different $PS_x$:$PFS_{1-x}$ ratios: (a) $PS_{1.0}PFS_0$, (b) $PS_{0.8}PFS_{0.2}$, (c) $PS_{0.6}PFS_{0.4}$, (d) $PS_{0.4}PFS_{0.6}$ and (f) $PS_{0.2}PFS_{0.8}$. In (e) and (g), zoom on the aggregates formed in the $PS_{0.4}PFS_{0.6}$ and $PS_{0.2}PFS_{0.8}$ films, respectively.. Scale bar: 20 µm.

Contact angle measurements of all the blended films as well as of films based on each separate component (i.e., PS, PFS and TIPS) were prepared following the same methodology

(**Figure S2**). The results indicate that the contact angle is influenced by the material nature and surface microstructure. Comparing the films based on PS, TIPS and TIPS:$PS_{1.0}PFS_0$, we observe that TIPS and TIPS:$PS_{1.0}PFS_0$ films show higher contact angles (98.4±0.7º and 96.3±0.8º, respectively) compared to films of only PS (88.6±0.7º). This points out that the OSC crystalline layer is on the top-surface and the polymeric layer is in contact with the $SiO_2$ dielectric, as previously reported.[33] This is in agreement with the AFM results. Similar high contact values are also observed with the PS:PFS based-blends. Time-of-flight secondary ion mass spectrometry (ToF-SIMS) of the films based on mixtures of PS and PFS further indicate that the PFS polymer is more concentrated far away from the $SiO_2$ interface, which is in agreement with the contrasted hydrophobic/hydrophobic character of these two materials (**Figure S3**).

With the aim at investigating how the incorporation of PFS affects the crystallization process of the films, we characterised the films by XRD (**Figure S4**). All the films exhibited only *(00l)* type reflections indicating that the crystallites in the thin films are highly oriented with the *ab* plane parallel to the substrate. The position and relatively intense diffraction peaks are in agreement with the known triclinic TIPS crystal structure.[33,38,42,43] Comparing the position of the first *(001)* peak, it can be observed that there is a small shift of up to 0.02º (from of 5.38º to 5.36º) when PFS is increasingly added. This might be indicative that the fluorinated polymer is introducing some lattice strain.[44]

The effect of the PFS on the OFET performance was explored by analysing the electrical properties of more than 20 devices per each formulation. All the devices were measured under environmental conditions. The transfer curves of the as-prepared films based on the different ink formulations are shown in **Figure 4** (black line) and their corresponding output characteristics are displayed in **Figure S5**. The presence of PFS in the blends clearly impacts on the electrical parameters, mainly threshold voltage ($V_{TH}$) and mobility (μ) (see **Table 1)**. Unexpectedly, the $V_{TH}$ undergoes a shift towards positive voltages when PFS is included in

the film composition. The devices with $PS_1PFS_0$ composition showed a $V_{TH}$ close to -1.2±0.3 V, while the ones based on $PS_{0.2}PFS_{0.8}$ exhibited a $V_{TH}$ close to 6.8±0.7 V. We believe that such $V_{TH}$ shift is due to certain *p*-doping of TIPS caused be the strong dipole moments of C-F bonds, which can lead to a downshift of the Fermi level of the OSC towards its HOMO level near the polymer/OSC interface.[45]

Regarding the field effect mobility in the saturation regime (μ), it decreased with increasing the proportion of PFS by one order of magnitude, from 0.7±0.1 $cm^2 \cdot V^{-1} \cdot s^{-1}$ for binary PS-based blend until 0.07±0.01 $cm^2 \cdot V^{-1} \cdot s^{-1}$ for the TIPS:$PS_{0.2}PFS_{0.8}$ films (**Table 1)**. This might be related with the reduction of the crystal domain size when PFS is included in the blend, as observed by AFM (**Figure 2**).

**Table 1**. Average OFET parameters measured in the saturation regime, and their standard deviation, extracted from devices prepared with the different blends. At least 20 devices (from 3 different coatings) have been prepared with each specific ink formulation.

| | $V_{TH}$ V | $\mu$ $cm^2 \cdot V^{-1} \cdot s^{-1}$ | $t_{1/2}$ s | $\beta$ | $\tau$ s |
|---|---|---|---|---|---|
| $PS_{1.0}PFS_0$ | -1.2±0.3 | 0.7±0.1 | (1.4±0.1)·$10^5$ | 0.27±0.02 | (2.4±0.2)·$10^5$ |
| $PS_{0.8}PFS_{0.2}$ | -0.3±0.2 | 0.46±0.06 | (6.2±0.1)·$10^5$ | 0.16±0.02 | (3.1±0.2)·$10^7$ |
| $PS_{0.6}PFS_{0.4}$ | 0.9±0.2 | 0.34±0.03 | (5.9±0.1)·$10^5$ | 0.18±0.02 | (5.8±0.2)·$10^6$ |
| $PS_{0.4}PFS_{0.6}$ | 3.0±0.1 | 0.22±0.02 | (5.5±0.1)·$10^5$ | 0.22±0.02 | (6.9±0.4)·$10^5$ |
| $PS_{0.2}PFS_{0.8}$ | 6.8±0.7 | 0.07±0.01 | (7.2±0.2)·$10^5$ | 0.31±0.03 | (6.3±0.3)·$10^4$ |

Previously in the literature, the stabilizing effects of PS have been reported, showing that PS helps to maintain the electrical properties of the devices for more than 50 days.[38,46] The shelf-stability of the transistors was studied here by measuring the devices for several months storing them in ambient conditions (**Figure 4 and Figure S6)**. The average life times ($t_{1/2}$) of the OFETs were estimated using a simple model of exponential decay (equation 1 and 2)[47]:

$$\mu(t) = \mu_0 \cdot e^{-kt} \qquad (1)$$

$$t_{1/2} = \frac{\ln(2)}{k} \qquad (2)$$

Equation 1 describes a simple model in which the mobility decreases following an exponential decay. From equation 2, the time required to decrease the OFET mobility to 50% of its initial value can be extracted.

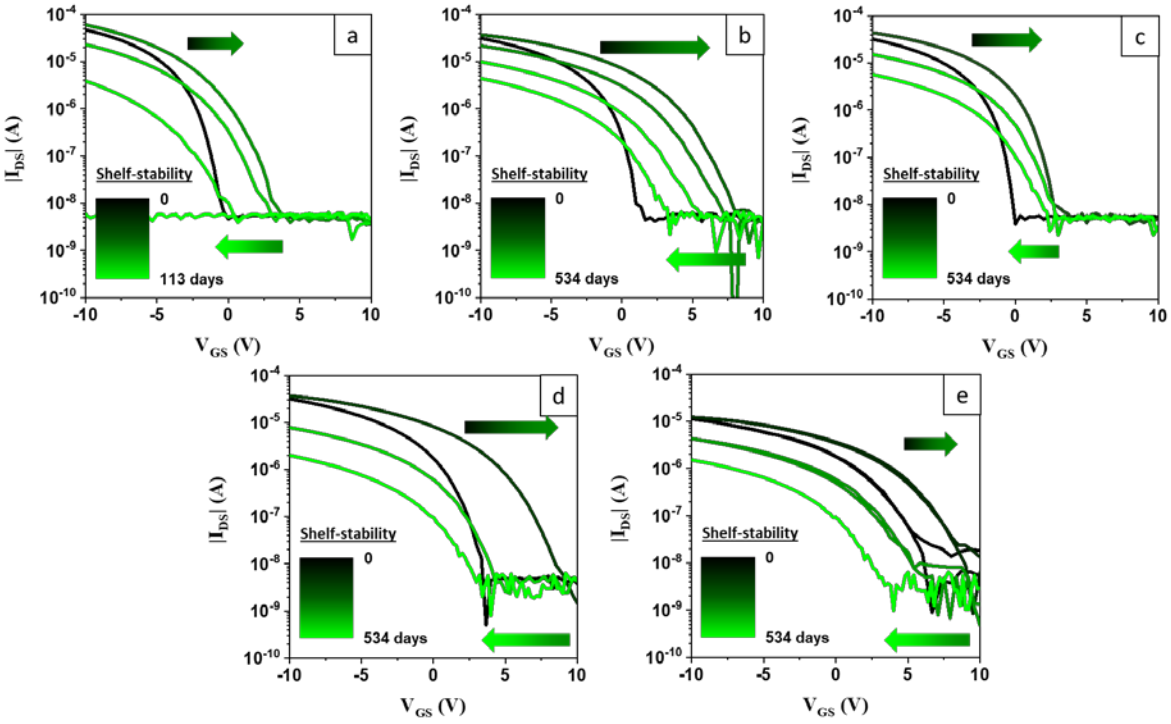


**Figure 4**. Transfer characteristics of TIPS:$PS_xPFS_{1-x}$ OFETs, as prepared and after different storage times in environmental conditions: (a) TIPS:$PS_{1.0}PFS_0$, (b) TIPS:$PS_{0.8}PFS_{0.2}$, (c) TIPS:$PS_{0.6}PFS_{0.4}$, (d) TIPS:$PS_{0.4}PFS_{0.6}$ and (e) TIPS:$PS_{0.2}PFS_{0.8}$.

Remarkably, $t_{1/2}$ of the TIPS:$PS_{1.0}PFS_0$ film was found to be 5 times lower than the blend films with fluorinated polymer (**Table 1**). The evolution of the $V_{TH}$ and the mobility with time is plotted in **Figure 5 (a-b)**. All the devices containing PFS showed a positive $V_{TH}$ shift the first ~40 days, followed by a negative shift and then after 120 days this parameter was stabilised. In terms of mobility, a fast decay of the saturation mobility was noted.

Nevertheless, the mobility of the films with fluorinated polymer also remained constant after the first 120 days. On the other hand, in the TIPS:$PS_{1.0}PFS_0$ OFETs a continuous mobility drop was found until the devices stopped working 113 days after their fabrication. The polarised optical microscopy images of the films registered 113 days after being prepared showed that the $PS_1PFS_0$ based films were not crystalline any more (**Figure S7)**. This was further corroborated by X-ray measurements, where XRD peaks were no longer discernible **(Figure S8)**. The loss of the TIPS thin film crystallinity was not reported before since its stability was usually monitored for shorter periods of time. However, the films with PFS did not exhibit any crystallinity deterioration. We attributed this effect to the penetration of humidity in the films containing only PS affecting the OSC crystals. In contrast, films that included PFS in their formulation, thanks to hydrophobic nature of this polymer, water was not importantly entering and damaging the OSC thin film.

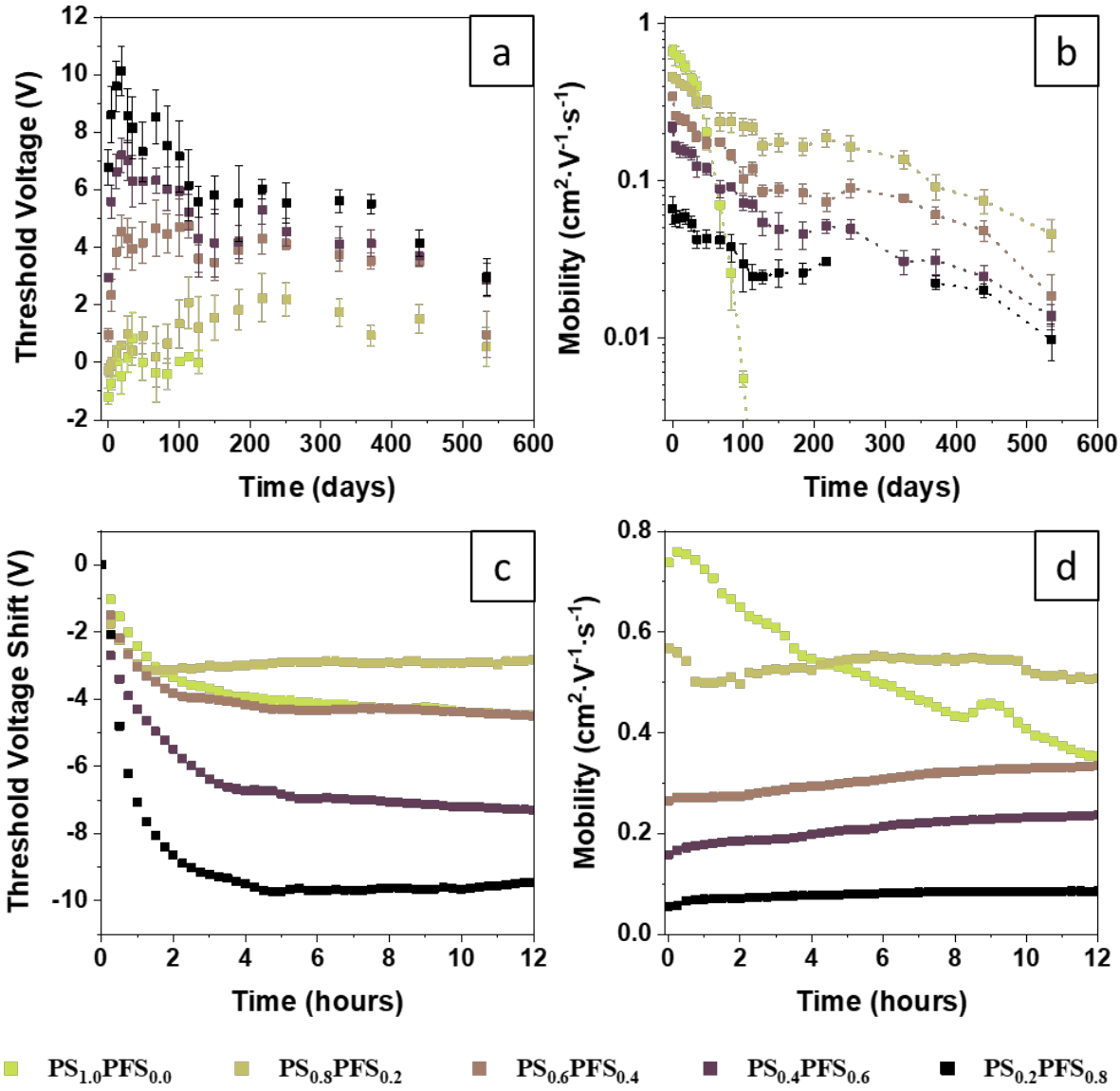


**Figure 5**. Evaluation of the shelf-stability measured over 500 days for TIPS:$PS_xPFS_{1-x}$ OFETs in terms (a) $V_{TH}$ and (b) $\mu^{sat}$ averaged from 8 devices. The saturation mobility was extracted at $V_{DS}$=−10 V. Bias stress stability measurements of TIPS:$PS_xPFS_{1-x}$ in terms of (c) threshold voltage shift and (d) $\mu^{sat}$ evolution during operation applying a $V_{GS}$ = -10 V and $V_{DS}$ = 0 V between the transfer measurements.

Subsequently, the bias stress of the devices under continuous operation was investigated. It should be highlighted that, in contrast to many reported works in which these measurements are performed under nitrogen ambient, here all the tests were carried out in ambient

conditions. The OFET bias stress is typically characterised by a $V_{TH}$ shift, which is related with the trapped charges at the dielectric/semiconductor interface or grain boundaries.[48–54] Obviously, the $V_{TH}$ shifts during $V_{GS}$ bias stress depends on the $V_{GS}$ and $V_{DS}$ applied.[55] $V_{GS}$ induces the formation of a density of charge carriers in the channel, while $V_{DS}$ moves the charges between source and drain.

The first measurements carried out consisted in applying a constant bias voltage $V_{GS}$ of -10 V and $V_{DS}$ of 0 V between each transfer measurement with an integration time of 10 s. Transfer characteristics were measured for 12 h every 15 minutes **(Figure S9).** The evolution of $V_{TH}$ and $\mu^{sat}$ with time is shown in **Figure 5(c-d).** Films with $PS_{0.8}PFS_{0.2}$ undergo a lower $V_{TH}$ shift around 3 V, while $PS_1PFS_0$ and $PS_{0.6}PFS_{0.4}$ presented a shift around 4 V, and $PS_{0.4}PFS_{0.6}$ and $PS_{0.2}PFS_{0.8}$ 6 and 8 V, respectively. Thus, a very low percentage of PFS in the blends improved the bias stress device stability, whereas a larger proportion of the fluorinated polymer turned to be detrimental. Considering the impact of the bias stress on the field-effect saturation mobility, it can be noticed that the films that contain PFS the saturation mobility loss is very small, while the $PS_1PFS_0$ films undergo a decrease in saturation mobility to almost half the original value after the experiment. The mobility drop during bias stress measurements is usually associated with an instability of the OSC due to charge trapping trap at the interface, water and oxygen absorption or changes in the crystal structure due to the field.[51,56,57] After a recovery process, the devices almost completely recovered their initial electrical properties, with the exception of the device with $PS_{0.2}PFS_{0.8}$ in which a slight electrical deterioration was observed (**Figure S10**).

The threshold voltage shift caused by the bias stress was fitted with the following Equation 3, which relates the threshold voltage shift with the concentration of traps:

$$\Delta V_{TH} = [V_{TH}(t=\infty) - V_{TH}(t=0)]\left(1 - e^{\left(-\frac{t}{\tau}\right)^{\beta}}\right) \qquad (3)$$

where t is the time, τ is the relaxation time for charge trapping, and β is the dispersion parameter related to the characteristic width of the band tail of the semiconductor.[55,58–60]

The values of these fitting parameters are shown in **Table 1**. For all the thin film formulations, the β value was in the range 0.15-0.30, which is of the same order as the values found for many previous bias stress experiments performed on p-channel devices.[61] Noticeably, the τ value of the $PS_{1.0}PFS_0$ and $PS_{0.4}PFS_{0.6}$ based film were of the order of $10^5$, whilst this parameter was of the order of $10^7$ for the $PS_{0.8}PFS_{0.2}$ and $10^6$ for the $PS_{0.6}PFS_{0.4}$ films. For the blends based on $PS_{0.2}PFS_{0.8}$ the τ value decreased even beyond the value found for the films based on only PS to the order of $10^4$. Considering these results, it can be concluded that the device bias stress is improved by addition of PFS in the blend, although the optimum performance is found with a percentage of the fluorinated polymer in the blend of 20% and above 40% of PFS the device stability and performance decreases.

Additionally, the bias stress experiment was repeated by applying also a $V_{DS}$ of -10 V in addition to a $V_{GS}$ of -10 V (**Figure S11-S12**). Under such stronger bias conditions, the threshold voltage shift potential was slightly higher than before (**Figure S13**). The β value increased to 0.20-0.35 and τ values were about one order of magnitude lower than the obtained with $V_{DS}$ = 0 V (**Table S2**). Nevertheless, the same effect of the PFS was found in this case.

Finally, the thin films were investigated employing a configuration of electrolyte-gated field-effect transistor (EGOFET). Its layout consists of exposing directly the OSC towards an electrolyte, where a gate contact is also immersed. The application of a source-gate voltage yields the formation of two electrical double layers (EDLs) at the gate/electrolyte interface and at the OSC/electrolyte interface. These EDLs determine the device electrical performance.[62,63] Typically, in EGOFETs water is used as electrolyte in order to apply these devices in biosensing.[64–67] However, one of their main drawbacks is the stability of the devices in such aqueous environment. Previously, we demonstrated that the use of OSC:PS blends leads to

EGOFETs with an improved stability. [68,69] Thus, here we investigated if such stability enhancement could be even increased by the addition of PFS in the blends.

The electrical performance of TIPS:$PS_xPFS_{x-1}$-based EGOFETs were measured in MilliQ water (**Figure S14**). The mobility of the devices decreased when the PFS load was higher than 20% from around 0.10 $cm^2/V{\cdot}s$ to 0.02±0.01 $cm^2/V{\cdot}s$ (**Table S3**). Only the TIPS:$PS_{0.2}PFS_{0.8}$ based EGOFETs did not resulted in a good modulation of the current, revealing a high degree of doping and difficulties to turn off the EGOFET. After stabilising the devices in MilliQ water, the devices were continuously monitored under operation. A $V_{DS}$ = -0.4 V (saturation conditions) was applied, while the $V_{GS}$ applied was selected to obtain an initial $I_{DS}$ of 1-2 µA (**Figure S15**). In all the cases, the $I_{DS}$ current decayed with time. However, the $t_{1/2}$ values, that is, the time that takes to reach 50% of the initial current value, were estimated to be 10, 36.4, 79.0 and 44.8 minutes for $PS_1PFS_0$, $PS_{0.8}PFS_{0.2}$, $PS_{0.6}PFS_{0.4}$ and $PS_{0.4}PFS_{0.6}$, respectively. Therefore, the hydrophobicity character of PFS also helped to avoid the diffusion of the ions into the films improving the device operational stability in aqueous media.

## 3. Conclusions

In conclusion, we demonstrated that adding a fluorinated polymer, such as PFS, in small molecules organic semiconductor/insulator polymer blends is an effective strategy to improve the OFET long term reliability. In particular, the addition of PFS in blends of the benchmark OSC TIPS with PS was here explored. Although the addition of PFS decreases the device mobility, we elucidated that finding a balanced PS:PFS ratio can provide additional appealing features regarding the overall device performance. By adding 20% of PFS, the films successfully operated for over one year and a half and exhibited a significantly improved bias stress stability. This was ascribed to the hydrophobic nature of the polymer that acts as barrier against humidity reducing hence charge trapping and deterioration of the crystalline films.

Our work advocates that the commonly employed route of using blends of OSCs with polymer binders to promote solution processability and thin film crystallinity, can be further exploited by adding fluorinated polymers to realise more reliable and stable devices without importantly compromising the device mobility.

## 4. Experimental Section

*Materials*: 6,13-Bis(triisopropylsilylethynyl)pentacene (TIPS, purity 97%) was purchased from Ossila and used without purification. Polystyrene (PS, 10000 $g \cdot mol^{-1}$), poly(pentafluorostyrene) (PFS), anhydrous chlorobenzene (CB, 99.8%) and 2,3,4,5,6-pentafluorothiophenol (PFBT; 97%) were purchased from Sigma Aldrich and used as received.

*Ink Formulation*: TIPS, PS and PFS were dissolved in anhydrous chlorobenzene (2.0 % wt.). The insulating polymer mixtures were prepared by mixing solutions at a volume ratio of 4:1, 3:2, 2:3, 1:4 Then, the TIPS:polymer ink was prepared by mixing the previous polymer mixture with pure TIPS solution at a volume ratio of 4:1.

*Device Fabrication*: Heavily p-doped Si wafers (Si-Mat) with a 200 nm-thick layer of $SiO_x$ thermally grown were used as substrates for the bottom gate bottom contact devices configuration and Kapton® foil (75 mm thick, DuPont) were used as substrates for the EGOFET configuration. Source and drain interdigitated electrodes were fabricated by photolithography and Cr (5 nm) and Au (40 nm) layers were deposited by vacuum thermal evaporation. The substrates were then cleaned in ultrasonic bath with acetone and isopropanol and then dried under nitrogen flow. The substrates were then treated with ultraviolet ozone for 25 min. Afterwards, the gold electrodes were chemically functionalized with a self-assembled monolayer of PFBT by immersing them in a 15 mM solution of PFBT in isopropanol for 15 min. The semiconductor layer was deposited on the substrates by using the BAMS technique as previously reported.[33,34]

*Electrical Characterization*: The OFET devices were measured with an Agilent B1500A semiconductor device analyser at ambient conditions. The organic devices were characterized extracting the field-effect mobility in linear ($V_{DS}$= -3 V) and saturation regime ($V_{DS}$=-10 V) and threshold voltage ($V_{TH}$). The channel length (L) of the devices was 25, 50, 100 and 200 µm and the width-length ratio (W/L) was 100. The SiO2 insulator capacitance per unit area (C) was 17.26 nF/cm$^2$. For each condition, the device parameters were extracted from more than 20 devices from 3 substrates to ensure thin film homogeneity and reproducibility.

The EGOFETs were measured with the Agilent B1500A semiconductor device analyser at ambient conditions employing MilliQ water as electrolyte and a gold wire as gate electrode. In the current monitoring experiments, the time between each point was of 5 seconds. The length (L) of the channel was 50 µm and the width-length ratio (W/L) was 100. For each condition, the device parameters were extracted from 8 devices from 2 substrates to ensure thin film homogeneity and reproducibility.

*Morphologic and structural Characterization*: Polarized optical microscope images and dark field microscope were taken using the Olympus BX51. The X-ray diffraction measurements were carried out with a D-5000 model Siemens diffractometer that used Cu K-alpha radiation 1.540560 Å. Surface topography, phase and thin film thickness were examined by a 5500LS SPM system from Agilent Technologies and subsequent data analysis was performed by using Gwyddion 2.43 software. Contact angle measurements were carried out with Drop Shape Analyzer DSA 100 from KRÜSS. The drop size was 4 µL of ultrapure water (18.2 MΩ·cm) and the measurements were repeated in 5 different places.

The vertical composition of the thin films were determined by ToF-SIMS analysis, surface sputter etching of the surface was accomplished with Cs beam, over a 300 µm × 300 µm area using 1 keV energy settings raster. A pulsed beam of 25 keV $Bi^{3+}$ ions scanned over a 50 µm × 50 µm region centered within the sputtered area was used. Analysis cycle time was 100 µs and sputtering cycle was 1 s and 500 ms flood gun compensation. A high current beam of low

energy (< 20 eV) electrons was employed for charge compensation, and negative ions were analyzed. The vacuum of the chamber was $1.7 \cdot 10^{-8}$ mbar.

**Supporting Information**
Supporting Information is available from the Wiley Online Library or from the author.

**Acknowledgements**
This work was funded by the Spanish Ministry with the project GENESIS PID2019-111682RB-I00 and through the "Severo Ochoa" Programme for Centers of Excellence in R&D (FUNFUTURE CEX2019-000917-S) and the Generalitat de Catalunya (2017-SGR-918). A. T. acknowledges his FPU fellowship and is enrolled in the UAB Materials Science PhD program.

**References**

[1] S. Riera-Galindo, A. Tamayo, M. Mas-Torrent, *ACS Omega* **2018**, *3*, 2329.

[2] Y. Diao, L. Shaw, Z. Bao, S. C. B. Mannsfeld, *Energy Environ. Sci.* **2014**, *7*, 2145.

[3] M. Nikolka, I. Nasrallah, B. Rose, M. K. Ravva, K. Broch, A. Sadhanala, D. Harkin, J. Charmet, M. Hurhangee, A. Brown, S. Illig, P. Too, J. Jongman, I. McCulloch, J. L. Bredas, H. Sirringhaus, *Nat. Mater.* **2017**, *16*, 356.

[4] X. Jia, C. Fuentes-Hernandez, C. Y. Wang, Y. Park, B. Kippelen, *Sci. Adv.* **2018**, *4*, eaao1705.

[5] H. F. Iqbal, Q. Ai, K. J. Thorley, H. Chen, I. McCulloch, C. Risko, J. E. Anthony, O. D. Jurchescu, *Nat. Commun.* **2021**, *12*, 2352.

[6] Y. Wang, X. Huang, T. Li, L. Li, X. Guo, P. Jiang, *Chem. Mater.* **2019**, *31*, 2212.

[7] F. C. Chen, C. H. Liao, *Appl. Phys. Lett.* **2008**, *93*, 103310.

[8] O. Acton, G. G. Ting, P. J. Shamberger, F. S. Ohuchi, H. Ma, A. K. Y. Jen, *ACS Appl. Mater. Interfaces* **2010**, *2*, 511.

[9] K. J. Baeg, A. Facchetti, Y. Y. Noh, *J. Mater. Chem.* **2012**, *22*, 21138.

[10] S. Casalini, C. A. Bortolotti, F. Leonardi, F. Biscarini, *Chem. Soc. Rev.* **2017**, *46*, 40.

[11] J. Kim, S. H. Kim, T. K. An, S. Park, C. E. Park, *J. Mater. Chem. C* **2013**, *1*, 1272.

[12] K. Kim, T. K. An, J. Kim, Y. J. Jeong, J. Jang, H. Kim, J. Y. Baek, Y. H. Kim, S. H. Kim, C. E. Park, *Chem. Mater.* **2014**, *26*, 6467.

[13] M. Jang, M. Lee, H. Shin, J. Ahn, M. Pei, J. H. Youk, H. Yang, *Adv. Mater. Interfaces* **2016**, *3*, 1600284.

[14] J. Kim, J. Jang, K. Kim, H. Kim, S. H. Kim, C. E. Park, *Adv. Mater.* **2014**, *26*, 7241.

[15] K. J. Baeg, D. Khim, J. Kim, H. Han, S. W. Jung, T. W. Kim, M. Kang, A. Facchetti, S. K. Hong, D. Y. Kim, Y. Y. Noh, *ACS Appl. Mater. Interfaces* **2012**, *4*, 6176.

[16] K. Kim, S. G. Hahm, Y. Kim, S. Kim, S. H. Kim, C. E. Park, *Org. Electron.* **2015**, *21*, 111.

[17] S. H. Kim, W. M. Yoon, M. Jang, H. Yang, J. J. Park, C. E. Park, *J. Mater. Chem.* **2012**, *22*, 7731.

[18] J. Granstrom, J. S. Swensen, J. S. Moon, G. Rowell, J. Yuen, A. J. Heeger, *Appl. Phys. Lett.* **2008**, *93*, 193304.

[19] H. Kim, D. H. Lien, M. Amani, J. W. Ager, A. Javey, *ACS Nano* **2017**, *11*, 5179.

[20] J. M. Kim, J. Oh, K. M. Jung, K. C. Park, J. H. Jeon, Y. S. Kim, *Semicond. Sci. Technol.* **2019**, *34*, 075015.

[21] M. Nikolka, G. Schweicher, J. Armitage, I. Nasrallah, C. Jellett, Z. Guo, M. Hurhangee, A. Sadhanala, I. McCulloch, C. B. Nielsen, H. Sirringhaus, *Adv. Mater.* **2018**, *30*, 1.

[22] S. Riera-Galindo, F. Leonardi, R. Pfattner, M. Mas-Torrent, *Adv. Mater. Technol.* **2019**, *4*, 1900104.

[23] L. J. Richter, D. M. Delongchamp, A. Amassian, *Chem. Rev.* **2017**, *117*, 6332.

[24] A. F. Paterson, N. D. Treat, W. Zhang, Z. Fei, G. Wyatt-Moon, H. Faber, G. Vourlias, P. A. Patsalas, O. Solomeshch, N. Tessler, M. Heeney, T. D. Anthopoulos, *Adv. Mater.*

**2016**, *28*, 7791.

[25] J. Smith, R. Hamilton, Y. Qi, A. Kahn, D. D. C. Bradley, M. Heeney, I. McCulloch, T. D. Anthopoulos, *Adv. Funct. Mater.* **2010**, *20*, 2330.

[26] C. E. Murphy, L. Yang, S. Ray, L. Yu, S. Knox, N. Stingelin, *J. Appl. Phys.* **2011**, *110*, 093523.

[27] J. Smith, R. Hamilton, I. McCulloch, M. Heeney, J. E. Anthony, D. D. C. Bradley, T. D. Anthopoulos, *Synth. Met.* **2009**, *159*, 2365.

[28] J. Smith, W. Zhang, R. Sougrat, K. Zhao, R. Li, D. Cha, A. Amassian, M. Heeney, I. McCulloch, T. D. Anthopoulos, *Adv. Mater.* **2012**, *24*, 2441.

[29] A. Pérez-Rodríguez, I. Temiño, C. Ocal, M. Mas-Torrent, E. Barrena, *ACS Appl. Mater. Interfaces* **2018**, *10*, 7296.

[30] K. Zhao, O. Wodo, D. Ren, H. U. Khan, M. R. Niazi, H. Hu, M. Abdelsamie, R. Li, E. Q. Li, L. Yu, B. Yan, M. M. Payne, J. Smith, J. E. Anthony, T. D. Anthopoulos, S. T. Thoroddsen, B. Ganapathysubramanian, A. Amassian, *Adv. Funct. Mater.* **2016**, *26*, 1737.

[31] A. Campos, S. Riera-Galindo, J. Puigdollers, M. Mas-Torrent, *ACS Appl. Mater. Interfaces* **2018**, *10*, 15952.

[32] Y. J. Jeong, D. J. Yun, S. Nam, J. Jang, *Appl. Surf. Sci.* **2019**, *481*, 642.

[33] I. Temiño, F. G. Del Pozo, M. R. Ajayakumar, S. Galindo, J. Puigdollers, M. Mas-Torrent, *Adv. Mater. Technol.* **2016**, *1*, 1600090.

[34] F. G. del Pozo, S. Fabiano, R. Pfattner, S. Georgakopoulos, S. Galindo, X. Liu, S. Braun, M. Fahlman, J. Veciana, C. Rovira, X. Crispin, M. Berggren, M. Mas-Torrent, *Adv. Funct. Mater.* **2016**, *26*, 2379.

[35] S. Galindo, A. Tamayo, F. Leonardi, M. Mas-Torrent, *Adv. Funct. Mater.* **2017**, *27*, 1700526.

[36] O. Yildiz, Z. Wang, M. Borkowski, G. Fytas, P. W. M. Blom, J. J. Michels, W. Pisula,

T. Marszalek, *Adv. Funct. Mater.* **2021**, 2107976.

[37] M. Berteau-rainville, A. Tamayo, T. Leydecker, A. Pezeshki, E. Orgiu, M. Mas-torrent, *Appl. Phys. Express* **2021**, *119*, 103301.

[38] I. Temiño, L. Basiricò, I. Fratelli, A. Tamayo, A. Ciavatti, M. Mas-Torrent, B. Fraboni, *Nat. Commun.* **2020**, *11*, 2136.

[39] Z. He, Z. Zhang, S. Bi, J. Chen, *Electron. Mater. Lett.* **2020**, *16*, 441.

[40] T. K. Kwei, T. Nishi, R. F. Roberts, *Macromolecules* **1974**, *7*, 667.

[41] T. Nishi, T. T. Wang, T. K. Kwei, *Macromolecules* **1975**, *8*, 227.

[42] S. C. B. Mannsfeld, M. L. Tang, Z. Bao, *Adv. Mater.* **2011**, *23*, 127.

[43] J. E. Anthony, D. L. Eaton, S. R. Parkin, *Org. Lett.* **2002**, *4*, 15.

[44] G. Giri, E. Verploegen, S. C. B. Mannsfeld, S. Atahan-Evrenk, D. H. Kim, S. Y. Lee, H. A. Becerril, A. Aspuru-Guzik, M. F. Toney, Z. Bao, *Nature* **2011**, *480*, 504.

[45] E. S. Shin, W. T. Park, Y. W. Kwon, Y. Xu, Y. Y. Noh, *ACS Appl. Mater. Interfaces* **2019**, *11*, 12709.

[46] L. Feng, W. Tang, J. Zhao, R. Yang, W. Hu, Q. Li, R. Wang, X. Guo, *Sci. Rep.* **2016**, *6*, 20671.

[47] H. J. Choi, C. A. Kim, J. I. Sohn, M. S. Jhon, *Polym. Degrad. Stab.* **2000**, *69*, 341.

[48] A. Sharma, S. G. J. Mathijssen, E. C. P. Smits, M. Kemerink, D. M. De Leeuw, P. A. Bobbert, *Phys. Rev. B - Condens. Matter Mater. Phys.* **2010**, *82*, 075322.

[49] G. Paasch, *J. Electroanal. Chem.* **2007**, *600*, 131.

[50] A. Street, A. Salleo, L. Chabinyc, *Phys. Rev. B - Condens. Matter Mater. Phys.* **2003**, *68*, 085316.

[51] R. A. Street, M. L. Chabinyc, F. Endicott, B. Ong, *J. Appl. Phys.* **2006**, *100*, 114518.

[52] M. Tello, M. Chiesa, C. M. Duffy, H. Sirringhaus, *Adv. Funct. Mater.* **2008**, *18*, 3907.

[53] A. Salleo, F. Endicott, R. A. Street, *Appl. Phys. Lett.* **2005**, *86*, 263505.

[54] J. B. Chang, V. Subramanian, *Appl. Phys. Lett.* **2006**, *88*, 233513.

[55] U. Zschieschang, R. T. Weitz, K. Kern, H. Klauk, *Appl. Phys. A Mater. Sci. Process.* **2009**, *95*, 139.

[56] R. A. Street, *Phys. Rev. B - Condens. Matter Mater. Phys.* **2008**, *77*, 165311.

[57] R. Di Pietro, D. Fazzi, T. B. Kehoe, H. Sirringhaus, *J. Am. Chem. Soc.* **2012**, *134*, 14877.

[58] H. Sirringhaus, *Adv. Mater.* **2009**, *21*, 3859.

[59] S. G. J. Mathijssen, M. Cölle, H. Gomes, E. C. P. Smits, B. De Boer, I. McCulloch, P. a. Bobbert, D. M. De Leeuw, *Adv. Mater.* **2007**, *19*, 2785.

[60] T. Jung, *J. Appl. Phys.* **2015**, *117*, 144501.

[61] F. Colléaux, J. M. Ball, P. H. Wöbkenberg, P. J. Hotchkiss, S. R. Marder, T. D. Anthopoulos, *Phys. Chem. Chem. Phys.* **2011**, *13*, 14387.

[62] L. Kergoat, L. Herlogsson, D. Braga, B. Piro, M. C. Pham, X. Crispin, M. Berggren, G. Horowitz, *Adv. Mater.* **2010**, *22*, 2565.

[63] L. Kergoat, B. Piro, M. Berggren, G. Horowitz, M. C. Pham, *Anal. Bioanal. Chem.* **2012**, *402*, 1813.

[64] Q. Zhang, A. Tamayo, F. Leonardi, M. Mas-torrent, *ACS Appl. Mater. Interfaces* **2021**, *13*, 30902.

[65] A. Kyndiah, F. Leonardi, C. Tarantino, T. Cramer, R. Millan-Solsona, E. Garreta, N. Montserrat, M. Mas-Torrent, G. Gomila, *Biosens. Bioelectron.* **2020**, *150*, 111844.

[66] S. Ricci, S. Casalini, V. Parkula, M. Selvaraj, G. D. Saygin, P. Greco, F. Biscarini, M. Mas-Torrent, *Biosens. Bioelectron.* **2020**, *167*, 112433.

[67] E. Macchia, K. Manoli, B. Holzer, C. Di Franco, M. Ghittorelli, F. Torricelli, D. Alberga, G. F. Mangiatordi, G. Palazzo, G. Scamarcio, L. Torsi, *Nat. Commun.* **2018**, *9*, 3223.

[68] Q. Zhang, F. Leonardi, S. Casalini, I. Temiño, M. Mas-Torrent, *Sci. Rep.* **2016**, *6*, 39623.

[69] F. Leonardi, S. Casalini, Q. Zhang, S. Galindo, D. Gutiérrez, M. Mas-Torrent, *Adv. Mater*. **2016**, *28*, 10311.